Bone 125 (2019) 61–73

Contents lists available at ScienceDirect

Bone

journal homepage: www.elsevier.com/locate/bone

Full Length Article

New insights into the process of osteogenesis of anosteocytic bone

Lior Ofer[a], Maitena Dumont[a], Alexander Rack[b], Paul Zaslansky[c], Ron Shahar[a,*]

[a] Koret School of Veterinary Medicine, The Robert H. Smith Faculty of Agriculture, Food and Environmental Sciences, The Hebrew University of Jerusalem, PO Box 12, Rehovot 76100, Israel
[b] ESRF - The European Synchrotron, CS40220, F-38043 Grenoble, France
[c] Department for Restorative and Preventive Dentistry, Charité – Universitaetsmedizin Berlin, 13353 Berlin, Germany

ARTICLE INFO

Keywords:
Anosteocytic bone
Osteogenesis
Osteocytes
Osteoblasts
Bone matrix

ABSTRACT

The bone material of almost all vertebrates contains the same cellular components. These comprise osteoblasts that produce bone, osteoclasts that resorb bone and osteocytes, which are the master regulators of bone metabolism, particularly bone modeling and remodeling. It is thus surprising that the largest group of extant vertebrates, neoteleost fish, lacks osteocytes entirely (anosteocytic bone).

Osteocytes are the progeny of osteoblasts, which become entrapped in the osteoid they secrete, then undergo several morphologic and functional changes, to finally form an intricate network of living cells in the bone matrix. While the process of osteogenesis of osteocytic bone has been thoroughly studied, osteogenesis of anosteocytic bone is less well understood. The current paradigm for formation of anosteocytic bone suggests that osteoblasts remain always on the external surface of the formed bone, and do not become entrapped in the osteoid. Such a process requires the osteoblasts to function in a fundamentally-different way from osteoblasts of all other bony vertebrates.

Here we present a comparative structural study of the osteocytic bones of zebrafish and anosteocytic bones of medaka and show that they are remarkably similar in structure at several hierarchical levels. Scanning electron microscopy and phase contrast-enhanced μCT reveal the presence of numerous mineralized objects in the matrix of anosteocytic bone. These objects resemble osteocytic lacunae in zebrafish bone, and their locations and distribution are similar to those of osteocytes in zebrafish bone.

Our findings provide support for the occurrence of a process of anosteocytic bone osteogenesis that has so far been rejected. In this process osteoblasts become entrapped in the bone matrix (as occurs in osteogenesis of osteocytic bone), but then undergo apoptosis, become mineralized and end up as part of the mineralized bone matrix.

1. Introduction

Bones are complex hierarchical structures, adapted to cope with a range of varying mechanical and metabolic functions. Their basic building blocks are mineralized collagen fibers consisting of carbonated hydroxyapatite nanocrystals and type 1 collagen nanofibers. The mineralized fibrils, together with non-collagenous proteins (NCPs) and water, form the bone matrix [1,2]. Bones also possess various cell types, including mesenchymally-derived osteoblasts (bone depositing cells), hematologically-derived osteoclasts (bone resorbing cells) and osteocytes. The latter are the most numerous cells of bones and are differentiated osteoblasts that become embedded within the extra-cellular matrix during the process of bone formation [3,4]. Osteocytes are believed to serve as mechanical sensors, and also function as regulators of bone repair (remodeling) and bone adaptation to load (modeling) [5–7].

The bones of all vertebrates form by two major processes of osteogenesis: intramembranous ossification and chondral ossification [8]. Intramembranous ossification occurs by direct bone deposition, while chondral ossification starts with a templating phase of a mesenchimally-derived cartilaginous *anlage*, which is then gradually either replaced by bone (endochondral ossification) or becomes surrounded by bone (perichondral ossification) [8]. Osteogenesis is an intricate process carried out by osteoblasts that secrete a precursor soft extracellular matrix, osteoid, composed mostly of type I collagen, which subsequently becomes mineralized. During osteogenesis, osteoblasts go through several developmental stages, and eventually either become buried in the mineralized matrix as osteocytes, or undergo programmed

* Corresponding author at: Laboratory of Bone Biomechanics, Koret School of Veterinary Medicine, The Robert H. Smith Faculty of Agriculture, Food and Environment, The Hebrew University of Jerusalem, Rehovot 76100, Israel.
E-mail address: Ron.shahar1@mail.huji.ac.il (R. Shahar).

https://doi.org/10.1016/j.bone.2019.05.013
Received 13 April 2019; Received in revised form 7 May 2019; Accepted 10 May 2019
Available online 11 May 2019

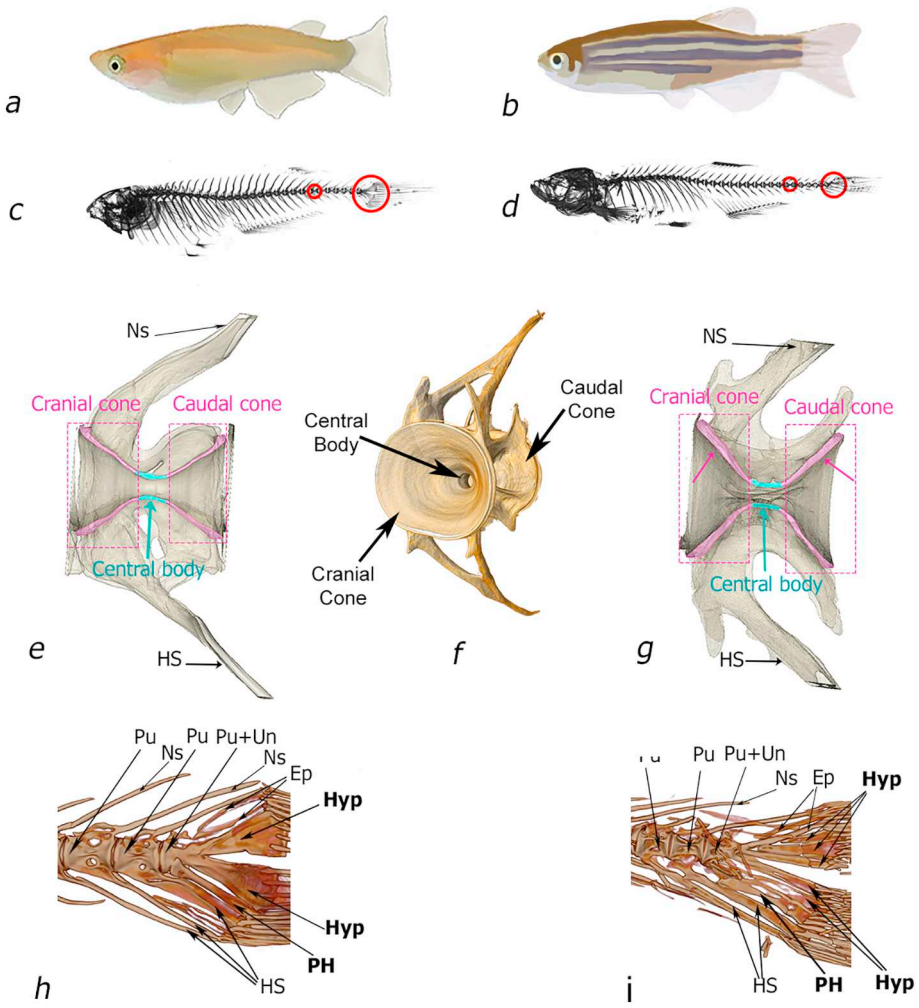

Fig. 1. Schematic representation of the bones studied in this manuscript. **a, b**. **Left:** medaka, **Right:** zebrafish **c, d**. The skeleton of medaka (a) and zebrafish (b). The smaller red circle shows the 4th caudal vertebrae and the large red circle shows the bones in the tail fin in the skeleton of medaka (c) and zebrafish (d). **e, g**. The different regions in caudal vertebrae are shown in longitudinal sections of medaka (e) and zebrafish (g) vertebrae. They include the cranial cone (marked in pink), the central body (marked in green) and the caudal cone (marked in pink). **f.** A 3-D image of a vertebra, showing the cranial and caudal cones, and the cylindrical central body connecting them. **h, i.** The different bones in the tail fin include the hypurals, parhypurals and epurals. They are shown here in the tail fin of both medaka (h) and zebrafish (i). Ep – epural, HS – haemal spine, Hyp – hypural, NS – neural spine, PH – parhypural, Pu – preural, Un – uroneural. (For interpretation of the references to colour in this figure legend, the reader is referred to the web version of this article.)

cell death or remain on the bone surface as bone lining cells [9–11]. The mechanism determining the ultimate fate of osteoblasts is largely unknown. Several theories have been proposed, including specific patterns of gene expression in certain osteoblasts, or cell response dictated by signals received from embedded osteocytes [10]. Once entrapped, osteoblasts undergo several morphological changes, transform into osteocytes and form a dense and intricate cellular network within the bone material. In the fully mineralized bone, osteocytes reside within small spaces called lacunae and communicate with their immediate neighbors and the external surfaces through cytoplasmic processes housed in narrow canals called canaliculi [3,4,12].

The bone material of the skeletons of fish is composed of the same basic building blocks as the skeleton of mammals and indeed all vertebrates [13,14]. Similar to bones of all other vertebrates, fish bones fulfill mechanical functions, ranging from anchoring muscles to maintaining the shape of the body and protection of internal organs [14–18]. The bones of all fish species contain osteoblasts and osteoclasts. However, surprisingly, the bones of almost all advanced teleosts (the majority of extant fish) completely lack osteocytes [14,19–21]. Since anosteocytic bone is restricted to advanced teleosts, while the bones of all other fish contain numerous osteocytes, the loss of osteocytes is considered a derived character within fish, resulting from a long evolutionary process [22]. Both osteocytic and anosteocytic fish inhabit a wide range of varied aquatic environments and are able to withstand prolonged, cyclic mechanical loads with high (similar to mammalian) strains throughout long lifespans [23]. Given the crucial role assigned to osteocytes in regulating bone modeling and remodeling, the complete absence of osteocytes in advanced teleosts is therefore intriguing. Nevertheless, the causes and consequences of the disappearance of osteocytes from the bones of advanced teleosts are still incompletely understood.

The process of osteogenesis of anosteocytic bones has so far been rarely studied, and better understanding may provide additional insights into osteoblast fate. Moss speculated more than half a century ago that anosteocytic bone may form either by continuous withdrawal of bone-producing osteoblasts from the newly-formed matrix, thus avoiding entrapment, or alternatively that osteoblasts do become entrapped within the bone matrix (as occurs in all other vertebrates), then die and become fully mineralized, thus resulting in anosteocytic bone [24]. More than two decades later, Weiss and Watabe [25] and Ekanayake and Hall [26,27] suggested that, in anosteocytic bones *'the osteoblasts recede from the mineralizing front and never become trapped as osteocytes'*. This observation was based on the fact that they could not find entrapped cells within the sections they studied. These reports form the basis for the currently prevailing paradigm of osteoblastic polarized secretion of bone matrix, namely that in anosteocytic bone of advanced teleosts osteoblasts secrete osteoid only towards the bone surface, thus avoiding entrapment.

Here we revisit the process of anosteocytic bone formation, using high-resolution 2D and 3D materials characterization methods. We compare micro-structural and cellular features in anosteocytic bones of medaka (*Oryzias latipes*) and osteocytic bones of zebrafish (*Danio rerio*). Our findings suggest that in the process of osteogenesis of anosteocytic bone osteoblasts do become entrapped in the bone matrix (as occurs in osteogenesis of osteocytic bone), but then die, become mineralized and end up as part of the acellular bone matrix. This process of anosteocytic

bone formation may occur instead of, or along with, the currently accepted paradigm of polarized secretion of bone matrix by osteoblasts.

2. Materials and methods

2.1. Fish

Adult (8–12 months old) medaka (*Oryzias latipes*, $n = 10$) and zebrafish (*Danio rerio,* n = 10) were obtained for this purpose from commercial fish suppliers (Aquatic Research Organisms, N.H., USA, and Aquazone, Israel, respectively). All medaka were male, while zebrafish consisted of both males and females. All medaka were from the same batch (hatched in the same month), 10 month-old fish, except for *in-situ* hybridization which was carried out on 12 month-old fish. Medaka were phenotypically very similar (their mean standard length was 28.05 ± 1.26 mm). Zebrafish were 8–12 months old and exhibited somewhat higher phenotypic variation in terms of length, due to their mixed population of males and females (mean standard length was 33.6 ± 2.47 mm). The fish were maintained in a controlled environment under a 12-h:12-h light:dark cycle at 28 °C, in accordance with standard guidelines, and fed appropriate commercial fish feed. All experiments were approved by the ethics committee of the Hebrew University of Jerusalem, permit # MD-16-14,844-3.

2.2. Bone samples

Bone samples were extracted from eight medaka and eight zebrafish that were euthanatized with an overdose of tricaine methane-sulfonate (MS-222; Sigma-Aldrich, USA). The caudal part of the vertebral columns, including the caudal fin (see Fig. 1 for details of these skeletal parts), were dissected and manually cleaned of soft tissue, using a stereo-dissection microscope. The harvested tissues were stored frozen at −20 °C until further processing, consisting of microtomography, polarized light microscopy and scanning electron microscopy. In addition, two medaka and two zebrafish were selected for histological sections and *in-situ* hybridization; they were euthanatized, their skin and scales were removed, and they were fixed in 4% paraformaldehyde (PFA/PBS) for 24 h at 4 °C, while being shaken gently.

2.3. Collagen orientation analysis by polarized light microscopy

The caudal vertebrae and tail sections of two medaka and two zebrafish were carefully cleared of soft tissue, avoiding damage to the vertebrae and caudal fin bones. Residues of soft tissue were removed by brief immersion in 3% hydrogen peroxide followed by washing with phosphate buffered saline (PBS). Sample birefringence was determined using an LC-PolScope polarization analysis image processing system (CRi, Inc., Woburn, MA, USA) mounted on a microscope (Nikon Eclipse 80i, Tokyo, Japan). Azimuth polarization orientations were determined and processed using the Abrio software tools (CRi, Inc., Woburn, MA, USA).

2.4. 3D imaging: High resolution phase contrast-enhanced μCT

The 4th caudal vertebra and fins of three medaka and three zebrafish were scanned using phase contrast-enhanced computed micro computed tomography (PCE- μCT) using inline propagation-based phase-contrast enhancement. Prior to imaging, each sample was mounted in a PVA vial, centrally stabilized in styropore-padded ethanol-saturated foam. Scans were performed on beamline ID19 of the European Synchrotron Radiation Facility (ESRF, Grenoble, France). An X-ray photon energy of 34 keV was used with an indirect X-ray imaging system combined with pco.edge (PCO, AG, Germany), with an effective pixel size of 650 nm. Each sample was mounted on the high-resolution rotation stage and a total of 4000 radiographic projections were recorded (200 ms exposures per angle) while continuously rotating the samples by 180°. Propagation- based X-ray phase-contrast enhancement was induced, using a sample-detector distance of 88 mm, to highlight internal voids and osteocytic lacunae. ESRF in-house code was used to reconstruct the data, enhancing contrast in the radiographs by means of Paganin-based filtering [28]. The reconstructed scans were segmented, then volume-rendered in 3D with Amira v.6.3 (Thermo Fisher Scientific, USA) and the mineralized tissue and voids were virtually separated. Volume-rendered lateral projection views of the cloud of osteocyte lacunae were segmented (for the cellular bones of zebrafish only), and were exported to imageJ. These images were used to analyze the orientation of each lacuna and produce orientation-colour-map, using the OrientationJ plugin.

2.5. Scanning electron microscopy

The caudal regions (caudal vertebral columns and caudal fins) of three medaka and three zebrafish were gradually dehydrated with increasing concentrations of ethanol, immersed for 8 h in solutions of polymethylmethacrylate (PMMA) followed by polymerization in an oven at 60 °C. The embedded bones were cut into *ca.* 0.5 mm thick transverse and longitudinal sections using an Isomet slow-speed water-cooled diamond-blade saw (Buehler, USA). The cut surfaces were ground with 3 μm and 1 μm grit *SiC* papers (Buehler, USA), followed by polishing with nap cloth soaked with diamond suspension (0.25 μm; Struers, USA). The polished samples were coated with gold and examined with scanning electron microscopes (JCM 6000 benchtop SEM and JEOL 7800 high resolution SEM; Jeol, USA) in secondary electron (SEI) and back scattered (BEI) modes with low and high vacuum and acceleration voltages of 5–15 kV.

2.6. Histology and In-Situ hybridization

For histology and *in-situ* hybridization two medaka and two zebrafish tails (after skin and scale removal) were fixed in 4% paraformaldehyde (PFA/PBS) for 24 h at 4 °C, while being shaken gently. After fixation, the tissues were decalcified for 24 h in 0.5 M EDTA pH 7.4, dehydrated in increasing concentrations of ethanol and embedded in paraffin. The embedded tissues were cut into 7 μm-thick sagittal sections, which were mounted onto glass slides. Hematoxylin and Eosin (H&E) staining was performed following standard protocols. The RNA probes for *in-situ* hybridization (ISH) were prepared by *in-vitro* transcription of the reverse transcriptase cDNA fragments, using T7 RNA polymerase. Fluorescence *in-situ* hybridization (FISH) was performed using fluorescein- labeled probes. FISH were performed following the protocol described in [29]. After hybridization, slides were washed, quenched and blocked. Hybridization probes for FISH were detected by incubation with peroxidase-conjugated anti-fluorescein antibody (anti-fluorescein- POD; Roche 1:200) followed by Cy3-tyramide-labeled fluorescent dyes according to the instructions of the TSA Plus Fluorescent Systems Kit (Perkin Elmer, USA). The following primers were used to generate the medaka col1a1 probe: forward-TGTT CCGTGCTGATGATGCT, reverse- ATGTACCGGTGTGTGACGTG. Col2a1 primers for *in-situ* hybridization probe generation were based on Dong et al. [30]: forward- GAATCAGCAAAGTACCAAAG, reverse- ACCGGC CTGAATGCCTCTT.

3. Results

3.1. Collagen orientation

Polarized light microscopy images of 4th caudal vertebrae of zebrafish (*D. rerio*) and medaka (*O. latipes*) reveal a remarkable similarity in their main collagen fiber orientations. In both species, the collagen fibers are oriented uniformly along the long axis of the neural and hemal spines, in a longitudinal orientation in the central body of the vertebra and in a circumferential orientation in the cranial and caudal

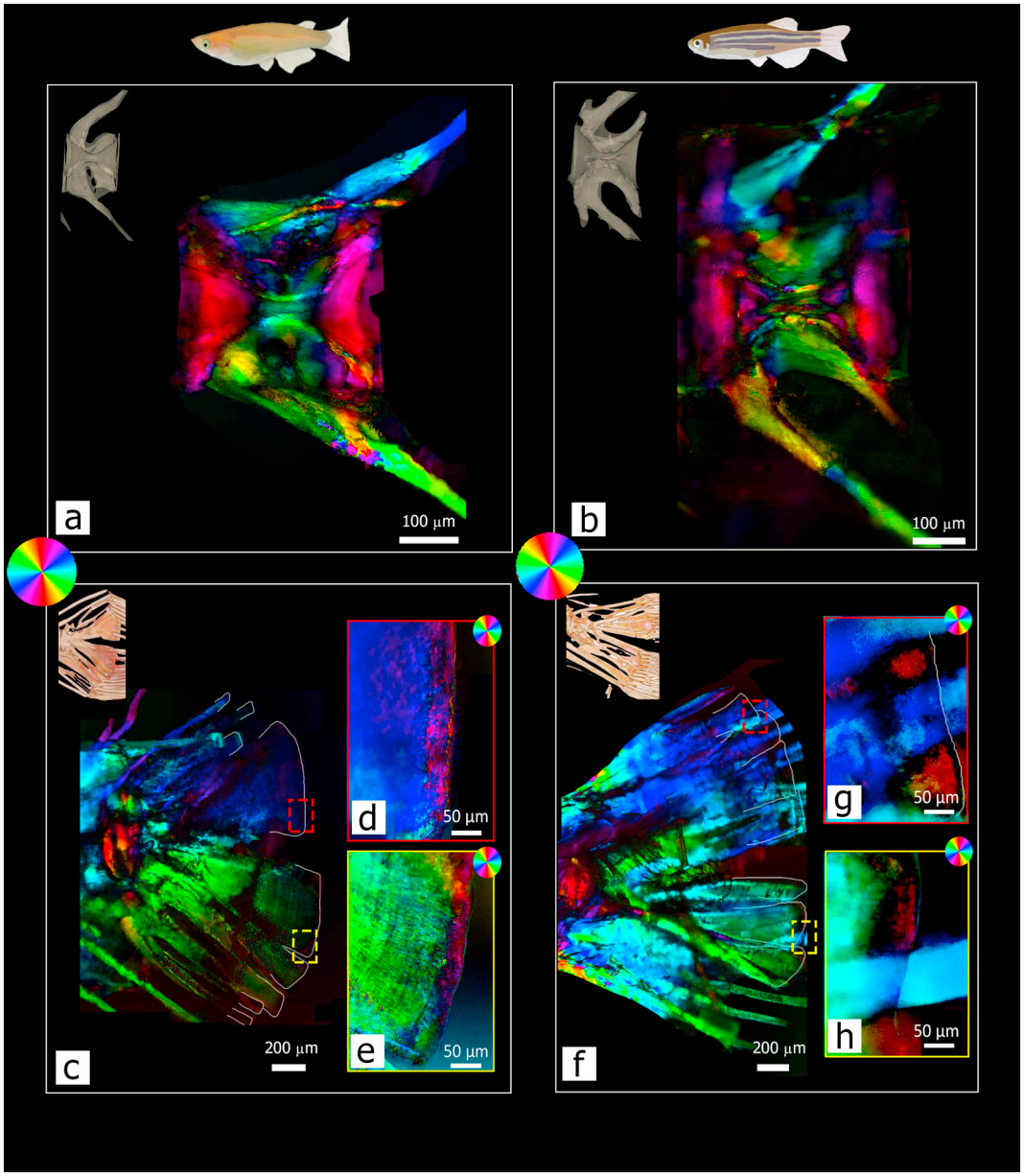

Fig. 2. Orientation of collagen fibers in the caudal vertebra and fin of zebrafish and medaka. **Left:** medaka, **Right:** zebrafish **a, b.** Collagen fiber orientation in the caudal vertebra (a, b) and tail bones (c, f) of medaka and zebrafish, respectively, identified by polarized light microscopy. The orientation of the collagen in both fish is remarkably similar. Notice the longitudinal orientation of the fibers along the vertebral spines, the longitudinally-oriented fibers in the middle part of the vertebra and the circumferentially-oriented fibers in the cranial and caudal vertebral cones (a, b). **c, f.** Tail fin bones of medaka (c) and zebrafish (f). The fibers are longitudinally oriented in the neural spines and in the hypurals parhypurals and epurals in the tail fins of medaka and zebrafish. Interestingly, a thin layer of collagen fibers, located in the most distal aspect of the tail bones (marked by the red and yellow rectangles) is oriented orthogonal to the long axis of these bones (see red patches in d, e, g, h). Circular colour wheels code angular orientations, such that each colour represents a directional vector and its 180^0 complement, as displayed in the colour wheel. (For interpretation of the references to colour in this figure legend, the reader is referred to the web version of this article.)

vertebral cones (Fig. 2a, b). Similar polarized light microscopy images were also obtained of the caudal fin skeleton of the two species, which contains neural spines, hypural, parhypural and epural bones (Fig. 2 c, f). The similarity of collagen orientation in these bones is once again very striking, with the collagen fibers aligned along the longitudinal axes of these bones. Interestingly, the collagen fibers in the caudal-most edges of the bones are oriented orthogonally to the longitudinal axis of the bone (see Fig. 2 d, e, g, h), in parallel with the surface osteoblasts which secreted them. It therefore follows that as the bone grows further in length, these collagen fibers must rotate by 90^0, to co-align with longitudinal axis of the bone, however the mechanism regulating this rotation is unclear.

3.2. Osteocytic lacunar orientation

Lacunar orientation analysis was performed in three vertebrae and tail fin bones of zebrafish and typical results are presented in Fig. 3. These orientation maps are directly comparable with the collagen orientation maps of the same bones presented in Fig. 2 b, f. The comparison reveals close similarity between the orientation of the collagen network and the orientation of the long axes of the ellipsoid osteocytic lacunae. Although the most caudal layer of osteocytes in the caudal fin diverges from the overall direction of the longitudinally oriented osteocytes, these cells maintain their close similarity to the collagen fiber orientation at this location (see Fig. 2 d, e, g, h).

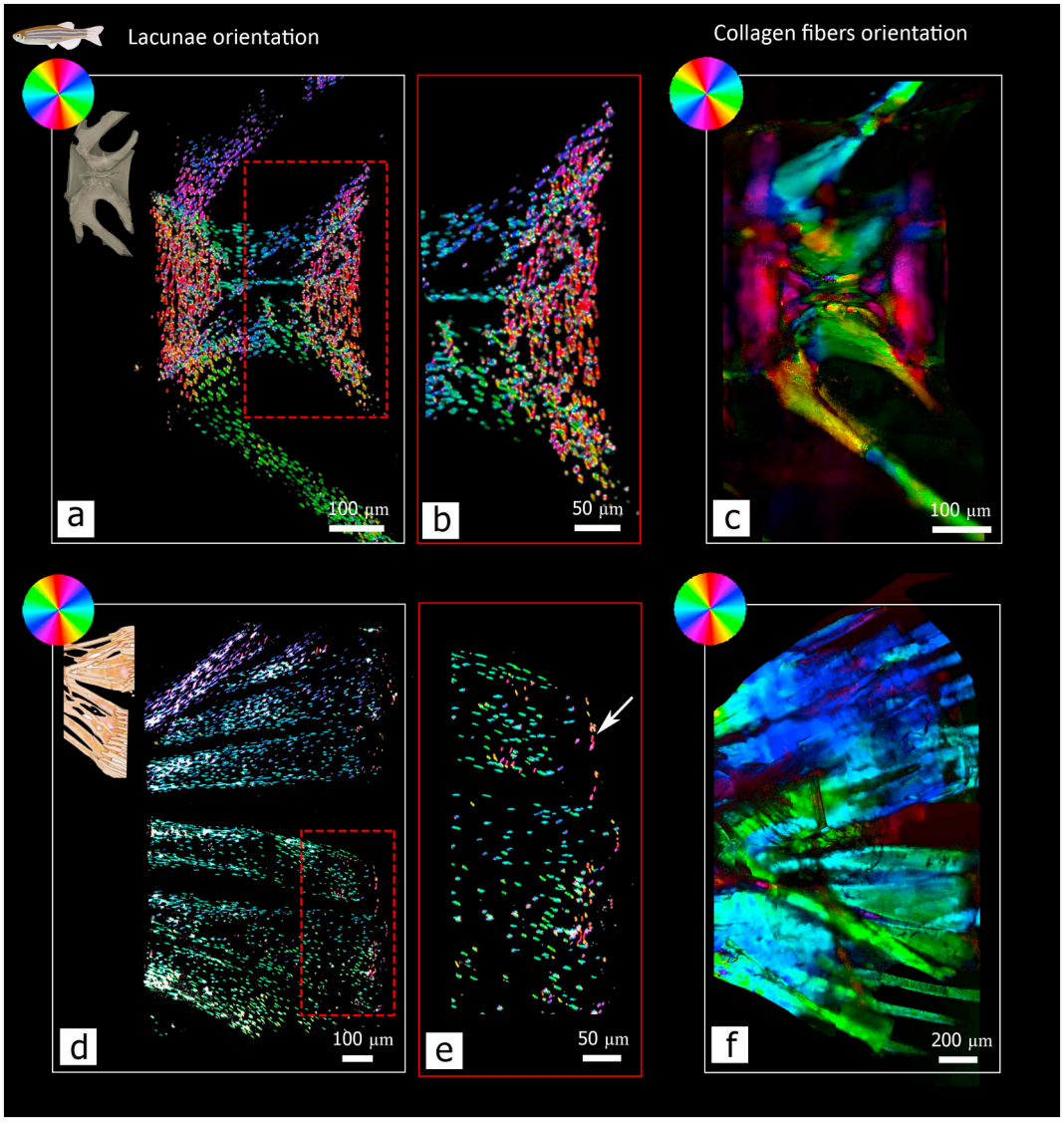

Fig. 3. Lacunae *versus* collagen orientation in the caudal vertebrae and caudal-fin bones of zebrafish. **a.** Lateral view of zebrafish 4th caudal vertebra, obtained from PCE-CT data, showing lacunar distribution and orientation. Notice the longitudinal orientation of the lacunae along the central body, and circumferential orientation in the cranial and caudal cones. **b.** Magnified view of the most caudal part of the caudal cone (area marked in (a) with a red rectangle). **c**. Lateral view of the same 4th caudal vertebra in (a) showing collagen orientation (see Fig. 2 b). **d.** Lateral view of the tail fin bones, showing lacunar distribution and orientation. Notice the longitudinal orientation of the lacunae along the neural spines, hypural epural and parhypural bones. **e.** Magnification of the caudal edge of the lower hypurals (red rectangle in d), showing that a thin layer of osteocytes in the most caudal aspect of this bone (arrow) is oriented orthogonal to the long axis of the hypurals. **f**. Lateral view of the same caudal fin showing collagen orientation. Circular colormaps code the angular orientation. (For interpretation of the references to colour in this figure legend, the reader is referred to the web version of this article.)

3.3. Location and position of osteoblasts

The arrangement of osteoblasts in the tail fin bones of medaka and zebrafish was examined by studying longitudinal histologic sections of medaka and zebrafish hypural bones, shown in Fig. 4. These bones comprise a cartilaginous core surrounded by bony collar [31], and their growth in length and width is achieved by surface apposition of mineralizing osteoid, termed perichondral ossification [32]. Close examination of these sections reveals that surface cells (likely osteoblasts, based on their morphology and location) at the proximal part of the bones are periostealy aligned along the long axis of the bone in both species (Fig. 4 b, e). At the distal surface, they are arranged with their long axes along the surface, so they are oriented orthogonal to the long axis of the bone (Fig. 4 c, f), in correlation with the collagen fiber and osteocyte orientation in this region (Fig. 2 d, h, g and 3 e). Some parts of the bone matrix in zebrafish seem to lack osteocytes (Fig. 4 e), while some parts of the bone matrix in the anosteocytic bone of medaka appear to contain osteocytes (Fig. 4 c).

In order to confirm that the cells lining the bony surface of the bones of the tail fin are osteoblasts and the core cells are chondrocytes, *in-situ* hybridization of Col1 (marker of mature osteoblasts) and Col2 (marker of mature chondrocytes) was performed on these sections. The cells on the surfaces of the hypural bone stained positively for Col1 and were thus positively identified as osteoblasts (see Fig. 5 b, c, d, e). *In-situ* hybridization using the Col2 marker of mature chondrocytes positively stained the cells of the cartilaginous core of the bone (Fig. 5 g, h, i).

3.4. Scanning Electron Microscopy and phase contrast-enhanced µCT

Transverse sections of the cranial and caudal cone regions of 4th caudal vertebrae of medaka were examined by complementary contrasts (secondary electrons, backscattered electrons, phase contrast-

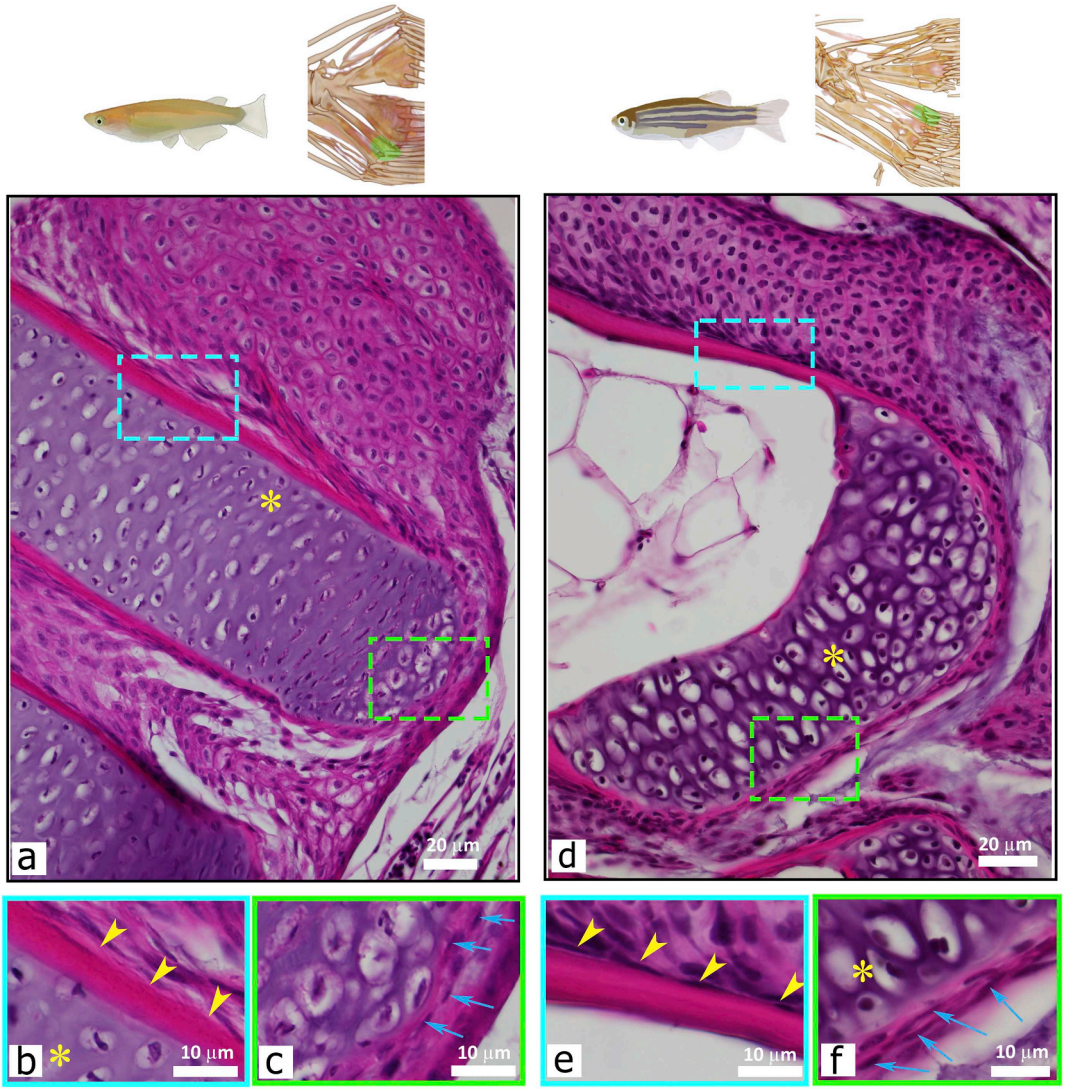

Fig. 4. H&E staining in the caudal-fin bones of medaka and zebrafish. **Left:** medaka, **Right:** zebrafish. Cartilage stains purple, bone stains red and muscle stains red-purple. The yellow asterisk marks the cartilaginous core of the bone in panels a, b, d and f. **a.** Medaka parhypural bone, longitudinal section, distal segment. The cartilaginous core is enveloped by a bony-collar. Two regions are marked by colored rectangles (blue and green) and are shown in b, c. **b.** Magnification of a proximal part of the bone. Yellow arrowheads show longitudinally-oriented osteoblasts on the surface of an anosteocytic bone collar. **c**. Magnification of the edge of the bone. Blue arrows show osteoblasts along the edge surface of the bone, thus orthogonally oriented to the long axis of the bone. **d.** Zebrafish hypural bone, longitudinal section, distal segment. **e.** Magnification of a proximal part of d, marked by a blue rectangle. Yellow arrowheads show longitudinally-oriented osteoblasts at the surface of the bony-collar. The bone appears to be anosteocytic. **f.** Magnification of the region marked by a green rectangle in d. Blue arrows show osteoblasts on the surface of the bone, and osteocytes within the bone matrix. We note that we refer here to cells within the bone matrix as osteoblasts until they complete the morphological changes characteristic of osteocytes, as detailed for example by Franz-Odendaal, Hall and Witten [9]. (For interpretation of the references to colour in this figure legend, the reader is referred to the web version of this article.)

enhanced μCT) (Figs. 6–7).

Scanning electron microscopy sections revealed the presence of numerous elliptically-shaped mineralized objects within the bone material, having similar shape and orientation to the osteocytic lacunae observed in similar sections of vertebrae of zebrafish (Fig. 6 a). In zebrafish, the distribution of the osteocytes is very clearly and sharply divided between two regions: the more interior region does not contain osteocytes at all, while the external region contains large numbers of a mixture of osteocytic lacunae and mineralized objects (Fig. 6 c, f, h). In medaka osteocytic lacunae are absent, but the spatial distribution and shape of the mineralized objects is very similar to the zebrafish lacunae. They are prominently present in the outer layer and completely absent from the inner layer(Fig. 6 a, d, g). Slices from phase contrast enhanced microCT scans of the 4th caudal vertebra of medaka and zebrafish show that while zebrafish sections (Fig. 6 l) contain, as expected, a large number of osteocytic lacunae, medaka sections (Fig. 6 k) are mostly homogeneous and without voids, with the exception of the outermost (and therefore most recently deposited) layer of the cones where numerous small voids are present, and may represent early stages of the osteoblastic mineralization process.

In order to validate these findings, sections of other parts of vertebrae and caudal fin bones of medaka were examined by scanning electron microscopy. Similar mineralized objects were also found in the hypural bones of the caudal fin of medaka (Fig. 7 a) and in the spines (Fig. 7 b), cone and 'arch attachment regions of medaka caudal vertebrae (Fig. 7 c). High magnification images of these objects, viewed using both secondary electron detector and backscattered electron detector show the shape of these objects and their orientation within the matrix (Fig. 7 d, e). The objects appear brighter than the matrix in images obtained by the backscattered electron detector (Fig. 7 d), suggesting they are more highly mineralized.

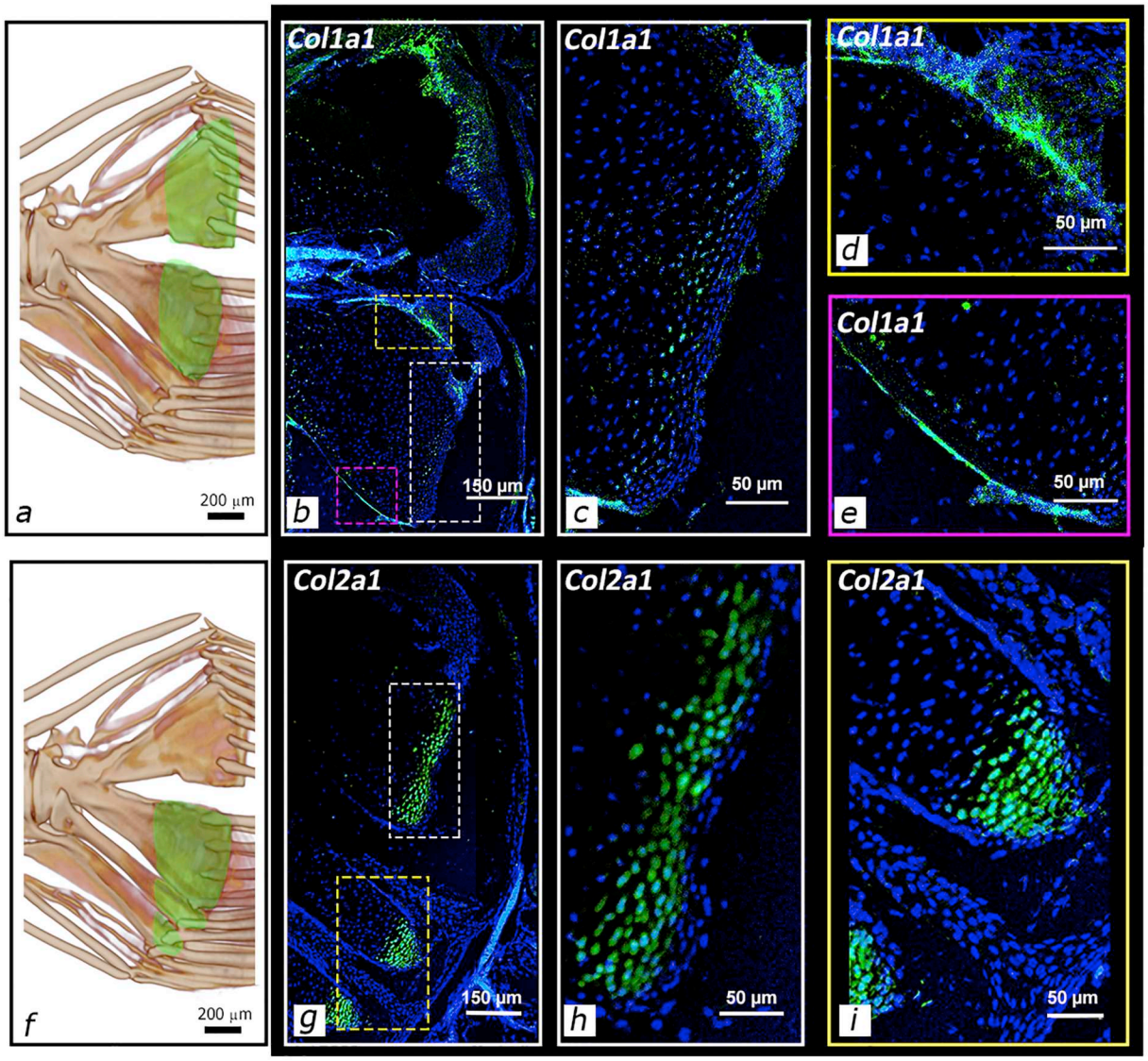

Fig. 5. *In-situ* hybridization and fluorochrome labeling in medaka hypurals. **a.** schematic showing medaka hypurals shown in the sections. **b.** Osteoblasts identified by Col1a1 *in-situ* hybridization (green). Squares (white, yellow and purple) mark the areas of magnifications (c, d and e, respectively) shown to the right. **c**. Magnification of the distal edge of the hypural bone. Thin layer of osteoblasts appears in green at the hypural edge. **d, e.** Magnifications of the more proximal parts of the bone. Mature osteoblasts expressing Col1a1 are located at the surface of the bone. **g.** Chondrocytes identification by Col2a1 *in-situ* hybridization (in green). Squares (white and yellow) mark the area of magnifications (h, i, respectively) shown to the right. **h, i**. Magnification of the edge of the hypural and parhypural bones. Col2a1-expressing chondrocytes are located at the edge of the cartilaginous core. (For interpretation of the references to colour in this figure legend, the reader is referred to the web version of this article.)

4. Discussion

Considering the pivotal role attributed to osteocytes, the occurrence of anosteocytic bone in the large and successful group of neoteleost fish leads to numerous questions. One of these questions concerned the process by which anosteocytic bone forms. While both osteocytic and anosteocytic bones are formed by osteoblasts, a fundamental difference must exist in the formation process of these two types of bone. This question appears to have been answered in a study published by Ekanayake and Hall, who reported that they could not find any evidence for the presence of either osteocytes or lacunae within the bone material of medaka vertebrae at any stage of the growth process [27]. They therefore concluded that osteoblasts of anosteocytic bones must secrete osteoid in a polarized manner, towards the bone surface only, and thus do not become trapped in the osteoid. This conclusion has since become the accepted paradigm of anosteocytic bone osteogenesis [4,27,33–34].

Since according to this paradigm the process of anosteocytic bone formation is inherently different from that of the process of osteocytic bone formation, the three-dimensional arrangement of the mineralized collagen fibrils in these two types of bone may differ as well. Although the osteoid of both bone types is secreted by the same cell type (osteoblasts), the presumed difference in their behavior in osteocytic bone (osteoblasts become entrapped and develop into osteocytes) and anosteocytic bone (osteoblasts avoid entrapment) may affect differently the three-dimensional arrangement of the collagen fibrils they secrete. It is of course also possible that collagen fiber orientation is controlled by local loads, in which case the process of osteogenesis will not influence collagen fiber orientation.

Lu and colleagues (2018), using live imaging of type I collagen assembly dynamics, provided some key insights into the process of osteoid production by osteoblasts [35]. Their study showed that each collagen type I fibril is the combined product of several osteoblasts, and that the secreted collagen does not diffuse far from the osteoblasts that

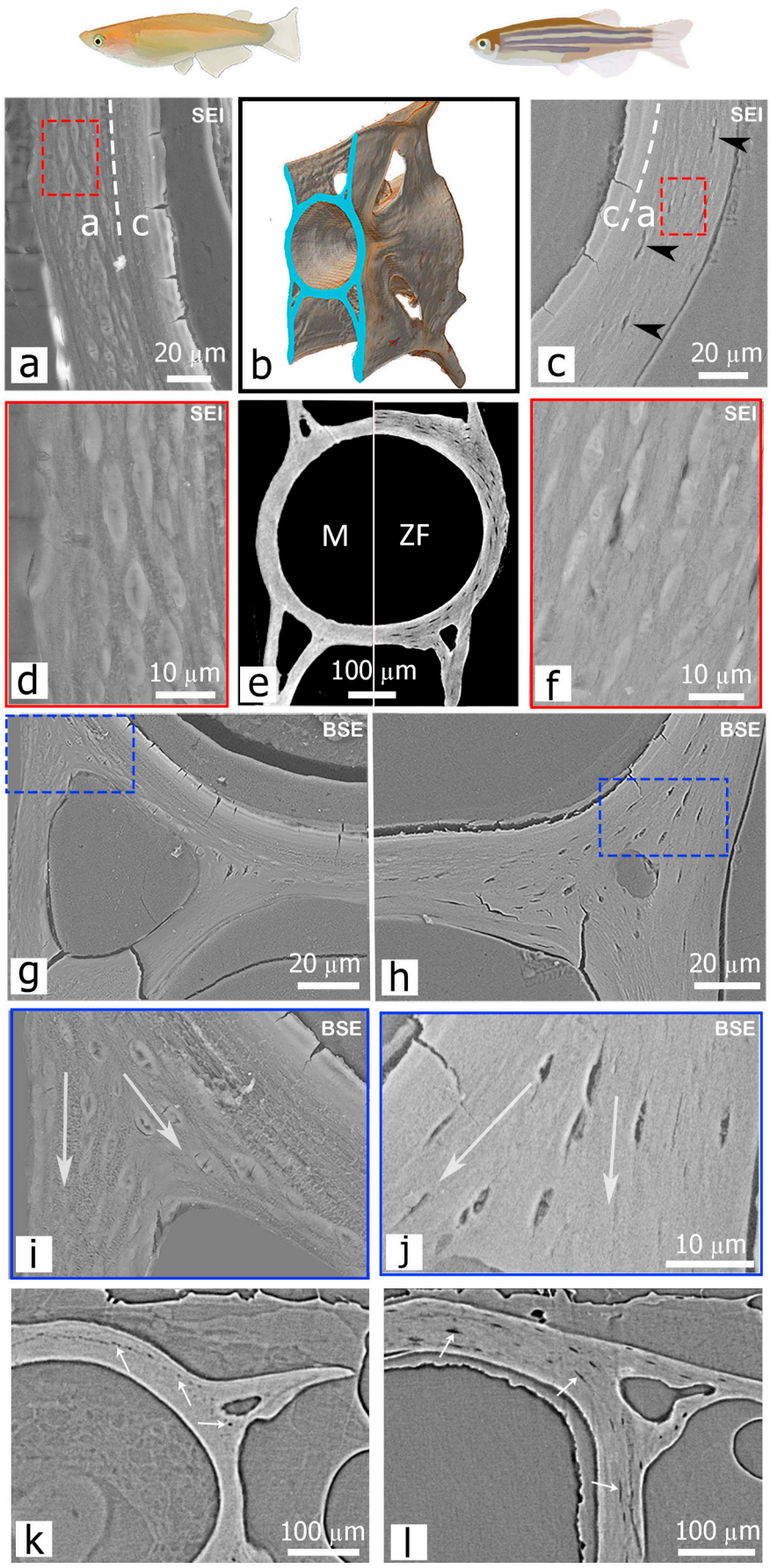

Fig. 6. Scanning electron microscope images of transverse sections of caudal vertebrae of medaka and zebrafish. **Left:** medaka, **Right:** zebrafish. **a.** SEM image of the lateral region of medaka vertebral centrum. **b.** 3D rendering of a vertebra, with the region of the transverse section marked in blue. **c.** SEM image of the lateral region of zebrafish vertebral centrum. In (a) and (c) two distinct regions are shown: c- chordacentrum, which is completely anosteocytic in both species, a- the autocentrum with osteocytic lacunae (black arrowheads in c) in the zebrafish and mineralized cell-like structures (shown in magnification in d, f) within circumferential layers in both species. Red squares mark the areas of magnifications shown in d and f. **d.** Mineralized objects of elliptical shape are seen within the bone matrix in medaka. **e.** Synchrotron tomography slices of complementary half-vertebra of medaka (left) and zebrafish (right). Notice the lack of lacunae in medaka as opposed to numerous lacunae in zebrafish **f.** Lacunae and mineralized lacunae within the bone matrix in zebrafish. **g, h.** SEM images of the regions of the attachment of the arch to the centrum of medaka (g) and zebrafish (h) vertebrae. Magnifications of the transition zone between the arch and the centrum of both medaka and zebrafish are shown in i and j, respectively. **i, j.** Mineralized objects in medaka (i) and osteocytic lacunae in zebrafish (j) occupy the autocentrum and not the chordacentrum. White arrows illustrate the orientation of the mineralized cells in medaka (i) and osteocytic lacunae in zebrafish (j). The pattern and organization of the mineralized objects in medaka match the arrangement of the osteocytic lacunae of the zebrafish, having a circumferential pattern at the centrum and longitudinal orientation along the arch. **k, l.** Slices from phase contrast enhanced microCT scans of the 4th caudal vertebra of medaka (k) and zebrafish (l). While the zebrafish section (l) contains, as expected, a large number of osteocytic lacunae (marked by arrows), the medaka section (k) is mostly homogeneous, without voids, except for numerous small voids (marked by arrows) that are mostly located in the outer layer of the cone and therefore likely to be the most recent layer deposited, and may represent incompletely mineralized lacunae. All SEM images were captured with high vacuum mode, at 15 kV. (For interpretation of the references to colour in this figure legend, the reader is referred to the web version of this article.)

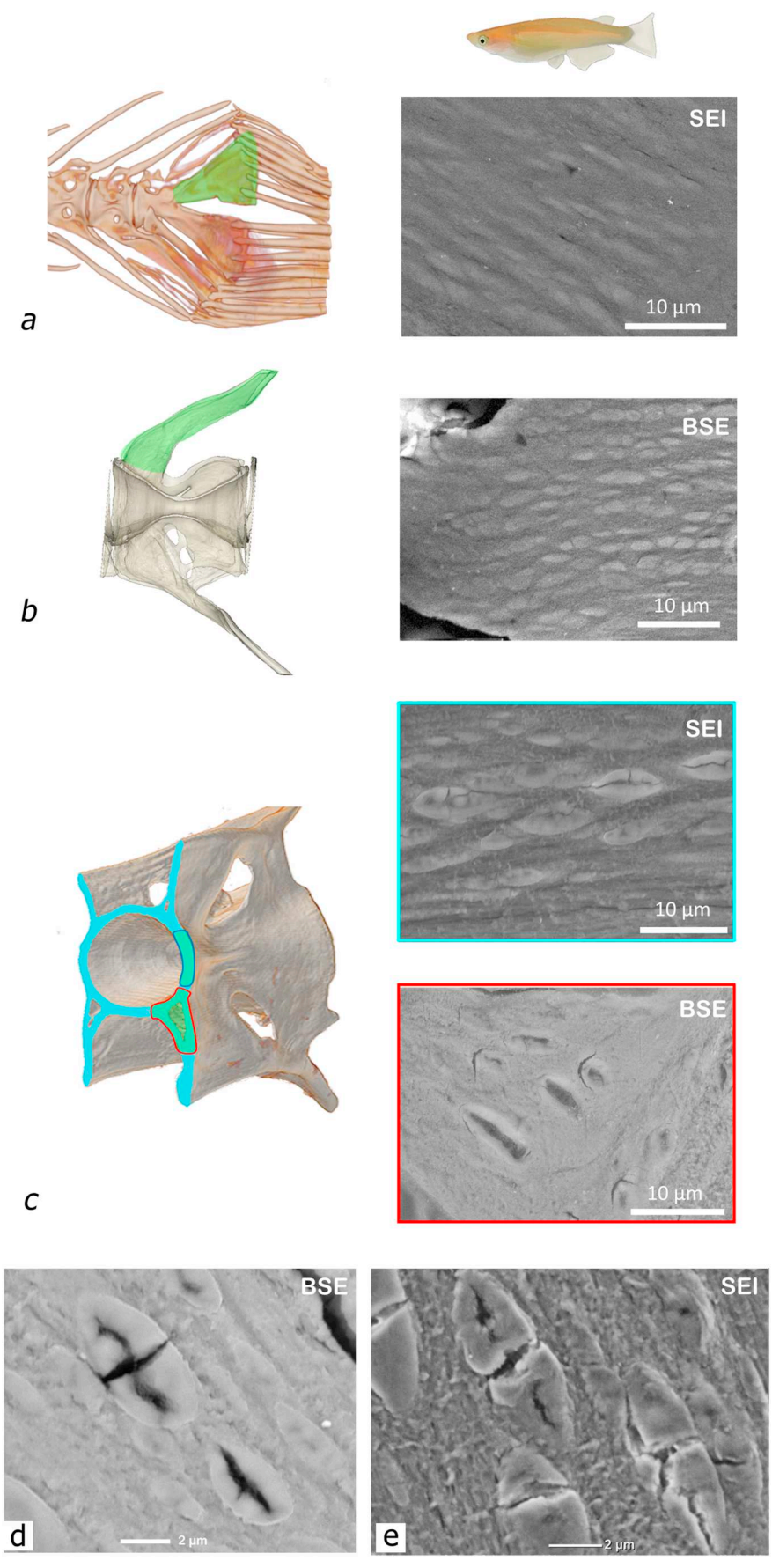

Fig. 7. Scanning electron microscope images of mineralized cells in selected areas of caudal fin and vertebral bones of medaka **a.** Mineralized objects within the matrix of the hypural bone in the tail fin of medaka. **b.** Mineralized objects aligned longitudinally within the matrix of the vertebral spine of medaka. **c.** Magnification of mineralized objects in the bone matrix in the cone and arch attachnent regions of vertebrae of medaka (marked in green in the schematic on the left). **d.** Mineralized objects viewed by scanning electron microscopy at 10 kV, using a back scattered detector. The objects seem hypermineralized compared to the surrounding matrix (brighter). **e.** Mineralized objects viewed by scanning electron microscopy at 5 kV, using a secondary electron detector. (For interpretation of the references to colour in this figure legend, the reader is referred to the web version of this article.)

produced it. The same study also showed that osteoblasts constantly move during collagen synthesis, exerting forces on the forming fibrils. Most interestingly, osteoblasts were found to be able to physically shape the collagen matrix by pushing collagen and forming 'holes' in the fibril network, creating room for osteocytic lacunae [35]. While these results are preliminary, they demonstrate the strong correlation between the mode of collagen secretion by osteoblasts and the arrangement of the fibrils they produce. Focused ion beam (FIB) studies in bones of several mammalian and fish species with acellular bone (*O. aureus*) led to the conclusion that bone consists of two different types of materials: [1] ordered arrays of collagen fibrils and [2] random and disordered arrangement of fibrils [1,17,36–39]. In these studies, the lacuno-canalicular system in the mammalian samples was consistently seen to be confined exclusively to the disordered material. It is thus likely that the presence of osteocytes, their lacunae and cellular extensions residing in the canaliculi, affects and interacts with the arrangement of the collagen, and in their absence, this arrangement may be different.

However, the results presented here show that collagen arrangement in osteocytic bones and anosteocytic bones is virtually identical. Specifically, polarized light microscopy images of the 4th caudal vertebrae of zebrafish (*D. rerio*, osteocytic bones) and medaka (*O. latipes*, anosteocytic bones) reveal a remarkable similarity of collagen fiber orientations, including similar orientational variations within the vertebrae (Fig. 2). Bones are formed either by intra-membranous ossification or by chondral ossification (endochondral or perichondral). The caudal vertebral bones of medaka and zebrafish are formed by intramembranous ossification [40,42]. Collagen deposition during intramembranous ossification is a rapid process, and the arrangement of the fibrils is considered to be less organized than collagen deposited during chondral ossification [35]. It is therefore theoretically possible that the similarity of collagen fiber orientations in osteocytic and anosteocytic vertebrae is limited to this type of bone ossification. However, similar collagen orientation was also seen in the neural spines, hypural, parhypural and epural bones of the caudal fin skeleton of the two species, which form by perichondral ossification [32]. While this high degree of similarity between collagen orientation in anosteocytic and osteocytic bones in both membranous and chondral bones certainly does not invalidate the assumed difference in osteoblast function in the process of osteogenesis, it is thought-provoking.

In mammals, the spatial distribution and alignment of the osteocytic network mirrors the organization of the collagen fibers of the extracellular matrix in which the cells are embedded [42–44]. Comparison of the lacunar orientation and collagen arrangement in zebrafish bones reveals a similar co-alignment. Such an alignment suggests that either the collagen matrix plays a significant role in defining the arrangement of the osteocytes, or that the arrangement of the osteocytes guides the orientation of the collagen fibers, or that both are determined by local load conditions. Since remarkable similarity was detected between collagen arrangement in bones of zebrafish (osteocytic bones) and medaka (anosteocytic bones), it is likely that the mechanism regulating their collagen orientation is also similar. Such similarity would rule out the possibility that osteocytes are responsible for collagen orientation. This leads to the conclusion that either collagen arrangement directs the orientation of the osteocytes, and is responsible for the co-alignment of osteocytes and collagen fibers, or that both collagen orientation and osteocyte orientation are determined by local load conditions.

It was demonstrated in mammals that formation of a highly oriented bone matrix, in terms of collagen and osteocyte arrangement, requires an alignment of osteoblasts that collectively build the matrix with long range order [44]. Since according to the paradigm of anosteocytic bone osteogenesis osteoblasts do not become entrapped in the osteoid, comparison of their position and orientation during osteoid secretion with osteoblasts involved in osteocytic bone formation is of interest. Evaluation of histological sections of bones of the tail fin of medaka and zebrafish reveals that the orientation and location of surface osteoblasts (positively identified by *in-situ* hybridization) was very similar in the bones of the two species (see Fig. 4). Furthermore, the orientation of surface osteoblasts mirrors the arrangement of collagen fibers in the bones of both medaka and zebrafish, as well as the arrangement of osteocytic lacunae in zebrafish. Histologic sections of the anosteocytic bone of medaka seem to show cells contained within the bone matrix, despite the fact that this matrix is supposed to be totally acellular (Fig. 4 c). At the same time, some regions of the bone matrix of zebrafish appeared anosteocytic (Fig. 4 e). We believe that the latter (absence of osteocytes in regions of osteocytic bone in zebrafish) is due to the combined effect of thin histological sections (7 μm) and relatively low density of lacunae in zebrafish bones. Therefore, a particular slice may pass through some lacunae, while missing others that happen to be below or above the plane of this slice, leading to absence of lacunae in parts of some slices. On the other hand, the presence of cells in the medaka bone matrix probably represents recently embedded osteoblasts prior to their death and subsequent mineralization.

The similarities between the various micro-structural and cellular elements of the bones of zebrafish and medaka (collagen orientation, osteoblast location and orientation, correlation of osteocyte orientation and collagen in zebrafish) merit further careful consideration. Though in themselves these observations do not necessarily contradict the existing paradigm of anosteocytic bone osteogenesis as described by Ekanayake and Hall [27], a re-evaluation of their findings seemed to be indicated. The methodologies used in the current study for this task consisted primarily of high-resolution scanning electron microscopy and phase contrast-enhanced μCT.

When transverse sections of the cone regions of caudal vertebrae of medaka were carefully examined by complementary, contrast-enhanced visualization techniques (secondary electrons, backscattered electrons, phase contrast-enhanced μCT), numerous mineralized objects were unexpectedly observed in this anosteocytic bone (Figs. 6 and 7). These objects were elliptical in shape, roughly 10 × 5 microns in size. They were consistently found in the outer half of the wall thickness of the conical elements of the caudal vertebrae of medaka (Fig. 6 a, g, i), and were always absent from the inner half of the thickness of cone wall. In terms of their 2D orientation, they were arranged with their long axes aligned circumferentially, similar to the orientation of collagen in the cones. The spatial distribution (location and orientation) of these mineralized objects is highly ordered and therefore cannot be the result of a random process. Furthermore, the mineralized objects were not limited to the vertebral cones of medaka. SEM images of hypurals, vertebral spines and the bases of the vertebral arches revealed that they are present in all these locations as well.

The sharp distinction observed in the location of the mineralized objects, between the inner and outer regions of the walls of the vertebral cones, can be linked to the unique process of vertebral development in teleosts. The vertebral centrum of the caudal vertebrae of adult teleosts forms initially as a notochordal structure by notochordal chordoblasts, which create a cylindrically-shaped bony layer within the notochordal sheath, called chordacentrum [45]. Following the formation of the chordacentrum, sclerotomal osteoblasts surround the chordacentrum and deposit cone-shaped intramembranous bone, the so-called autocentrum [46,47]. It thus appears that the presence of the mineralized objects is limited to those parts of the vertebrae that are created by osteoblasts (autocentrum) while the inner chordacentrum, created by chordoblasts, lack them entirely. It should also be noted that while the vertebral arches, spines and the outer half (autocentrum) of the caudal vertebrae of medaka are formed by osteoblasts through the process of intramembranous ossification, the hypural bones of the caudal fin form by perichondral ossification. Thus, the presence of these mineralized objects is not limited to a particular type of bone formation, and occurs in all bone matrices deposited by osteoblasts.

Comparison of similar sections in caudal vertebrae of zebrafish and medaka revealed a remarkable similarity between osteocytic lacunae in zebrafish and the mineralized objects in medaka (see Fig. 6). This

similarity was noted in size, shape, orientation, distribution and overall appearance. Specifically, we found presence (and absence) of lacuna-like mineralized objects (medaka) and lacunae (zebrafish) in the same locations within the vertebrae, so that they are present in bone deposited by osteoblasts, but absent from bone deposited by chordoblasts. These findings suggest that the current paradigm of osteogenesis of anosteocytic bone may need to be revised.

Based on our findings, we propose an alternative process of anosteocytic bone formation, which may occur instead of, or along with, the currently accepted process. We suggest that anosteocytic bone osteogenesis start off in much the same way as osteocytic bone formation. Specifically, osteoblasts secrete osteoid, then become immersed in osteoid (either osteoid they secreted or osteoid secreted by their neighbors). At this stage mineralization of the osteoid begins, regulated by a mechanism that is not fully understood. In osteocytic bones the mineralization process is coupled with morphologic and metabolic changes in the buried osteoblasts, that guide their transformation into osteocytes and the creation of the lacuna-canalicular system. The regulation of this process is complex and intricate, as it must ensure the health of live cells in a stiff and mineralized environment. However, in anosteocytic bones this regulatory mechanism can either be shut off or changes to actively lead to death of these cells, followed by their progressive mineralization and finally the mineralization of the entire lacunar space, so that it smoothly merges with the surrounding matrix. This concept seems to be simpler than the polarized osteoblast secretion theory, since it does not require the entire machinery of osteoblast function to change radically. Rather, the difference between the two paths is mainly that in anosteocytic bones the protective apparatus responsible for allowing the osteocytes to survive in the fully mineralized matrix and avoid being mineralized is turned off. Our proposal for the differences between the process of osteogenesis in osteocytic and anosteocytic bones is described schematically in Fig. 8.

Occasionally, but rather rarely, single unmineralized osteocyte-like structures can be seen in medaka bones, at the same locations and with the same directionality as the mineralized objects and the osteocytes of zebrafish in equivalent locations (Fig. 4 c). These osteocyte-like structures were found at the distal edge of the forming bone, nearest to the location of active bone deposition. These findings suggest that during anosteocytic bone formation osteoblast entrapment, apoptosis and mineralization are a continuous process that includes a transient pre-mineralization stage that can be seen in few locations at each time point. This observation is supported by the images produced of sections of vertebrae obtained from phase contrast-enhanced nano-tomography, which show small voids mostly in the outermost layers in medaka vertebral cones (Fig. 6 k). We also note that osteocytic lacunae in various stages of mineralization were observed in the osteocytic bones of zebrafish (Fig. 6 c, f). Mineralization of osteocytes, manifested as small calcified nano-spherites within osteocytic cell bodies, was reported by several authors in aged human bone and was termed micropetrosis [48,49]. This mineralization process could possibly progress to cell death and complete mineralization. While in that report the process was associated with pathologic changes of aging, in fish with anosteocytic bones, and to a more limited extent in bones of osteocytic fish, this may be a normal pathway.

The findings presented here are descriptive and provide only circumstantial evidence for the process of anosteocytic bone osteogenesis we propose, and definitive validation will require further studies. For example, cell fate studies, using marked osteoblasts and following them dynamically *in vivo* during osteogenesis could confirm whether they indeed become embedded in osteoid, then die, mineralize and become part of the matrix. Other advanced molecular techniques, such as apoptosis assays could not only confirm the assumption made here, that the buried osteoblasts undergo programmed cell death, but also allow the determination of the exact cellular stage at which this happens.

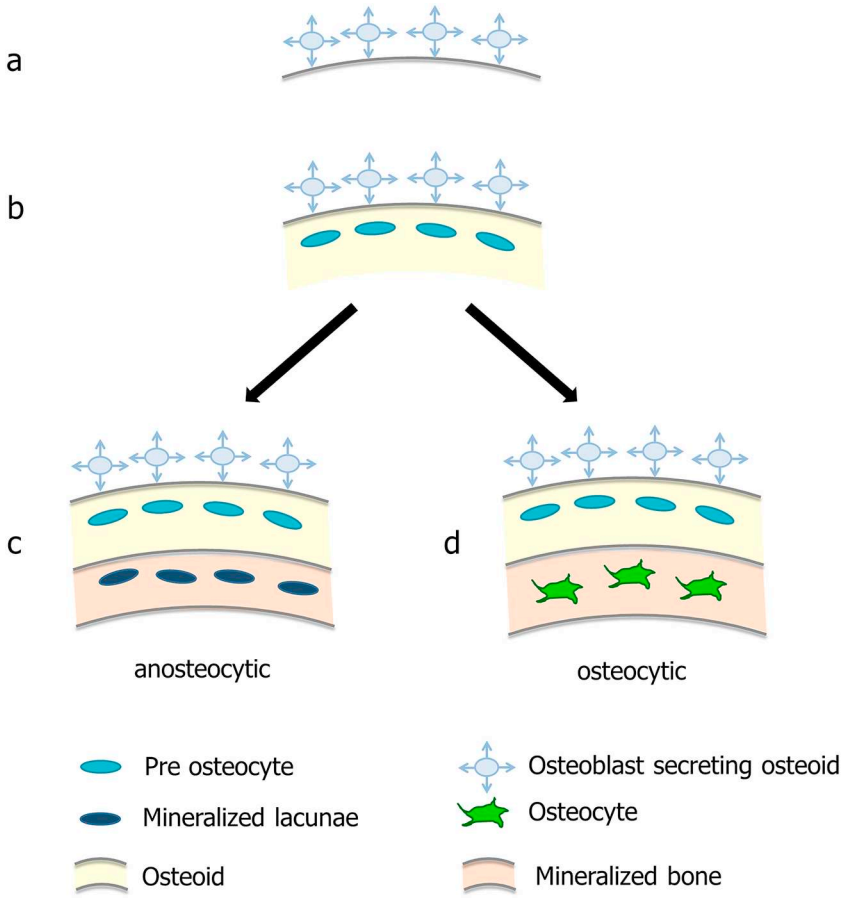

Fig. 8. Schematic description of the proposed process of osteogenesis in osteocytic and anosteocytic bone **a.** Osteoblasts on the bone surface produce osteoid. **b.** The osteoblasts that produced the osteoid become embedded within it, and a new layer of surface osteoblasts forms on the new bone surface. **c.** In anosteocytic bone the osteoid mineralizes and the buried osteoblasts undergo apoptosis and become mineralized as well. The osteoblasts that secreted the new osteoid layer become embedded, and a new layer of osteoblasts forms on the new bone surface. **d.** In osteocytic bone the osteoid becomes mineralized, buried osteoblasts become osteocytes, the osteoblasts that sectreted the new layer of osteoid become embedded, and a new layer of osteoblasts forms on the new bone surface.

Such studies are however beyond the scope of the current study.

In summary, the results presented here show circumstantial evidence to the occurrence of a process of anosteocytic bone osteogenesis, in which osteoblasts secrete bone, then become trapped in their secretions, die and mineralize. Such a process may occur alone or together with the currently accepted paradigm of polarized matrix secretion by osteoblasts. It is yet unknown, though, why osteoblasts die and become mineralized in anosteocytic bone, in contrast to osteoblasts that stay alive, become osteocytes and reside inside lacunae in osteocytic bones.

Acknowledgements

We are grateful to all members of the Zelzer group (particularly Dr. Yulia Shwatz and Shiri Kult) for technical support with various molecular methods; Katrein Sauer for assistance with phase contrast-enhanced μCT scanning; Birgit Schonert for help with sample preparation. Beam time (I.D. 19) was provided by the European Synchrotron Radiation Facility (ESRF). LO, PZ and RS were supported by the German Research Foundation (DFG), grant DFG GZ 577/5-1.

Author contribution

LO and RS designed the study; LO and RS performed immunohistochemistry and histology; LO, PZ, RS acquired microscopy images; LO, PZ and AR performed synchrotron PCE-CT measurements and processed 3D data; LO and RS quantified data; LO, MD and RS created figures; LO, MD, PZ and RS prepared the manuscript; all authors read and approved the manuscript.

Competing interests

The authors declare no conflict of interest.

References

[1] N. Reznikov, R. Shahar, S. Weiner, Bone hierarchical structure in three dimensions, Acta Biomater. 10 (2014) 3815–3826.
[2] S. Weiner, H.D. Wagner, The material bone: structure-mechanical function relations, Annu. Rev. Mater. Sci. 28 (1998) 271–298.
[3] L.F. Bonewald, The amazing osteocyte, J. Bone Miner. Res. 26 (2) (2011) 229–238 20.
[4] T.A. Franz-Odendaal, B.K. Hall, P.E. Witten, Buried alive: how osteoblasts become osteocytes, Dev. Dyn. 235 (2005) 176–190.
[5] L.F. Bonewald, The role of the osteocyte in bone and nonbone disease, Endocrinol. Metab. Clin. N. Am. 46 (2017) 1–18.
[6] J.-H. Chen, C. Liu, L. You, C.A. Simmons, Boning up on Wolff's Law Mechanical regulation of the cells that make and maintain bone, J. Biomech. 5 (43) (2010) 108–118.
[7] S. Tatsumi, K. Ishii, N. Amizuka, M. Li, T. Kobayashi, K. Kohno, M. Ito, S. Takeshita, K. Ikeda, Targeted ablation of osteocytes induces osteoporosis with defective mechanotransduction, Cell Metab. 5 (2007) 464–475.
[8] Francillon-Vieillot H, De Buffrénil V, Castanet J, Geraudie J, Sire J-Y, Zylberberg L, de Ricqles A. Microstructure and mineralization of vertebrate skeletal tissues. In: Carter JG, (Ed.) Skeletal Biomineralization: Patterns, Processes and Evolutionary Trends. American Geophysical Union; pp. 471–522.
[9] T.A. Franz-Odendaal, B.K. Hall, P.E. Witten, Buried alive: how osteoblasts become osteocytes, Dev. Dyn. 235 (2005) 176–190.
[10] S.L. Dallas, L.F. Bonewald, Dynamics of the transition from osteoblast to osteocyte, Ann. N. Y. Acad. Sci. 5 (1192) (2010) 437–443.
[11] M. Capulli, R. Paone, N. Rucci, Osteoblast and osteocyte: games without frontiers, Arch. Biochem. Biophys. 561 (2014) 3–12.
[12] L. Cao, T. Moriishi, T. Miyazaki, T. Iimura, M. Hamagaki, A. Nakane, Y. Tamamura, T. Komori, A. Yamaguchi, Comparative morphology of the osteocyte lacunocanalicular system in various vertebrates, J. Bone Miner. Metab. 29 (2011) 662–670.
[13] J.M. Horton, A.P. Summers, The material properties of acellular bone in a teleost fish, J. Exp. Biol. 212 (2009) 1413–1420.
[14] M.N. Dean, R. Shahar, The enigmas of bone without osteocytes, BoneKEy Reports 2 (2013) 1–8.
[15] A. Atkins, M.N. Dean, M.L. Habegger, P.J. Motta, L. Ofer, F. Repp, A. Shipov, S. Weiner, J.D. Currey, R. Shahar, Remodeling in bone without osteocytes: billfish challenge bone structure-function paradigms, Proc. Natl. Acad. Sci. U. S. A. 111 (2014) 16047–16052.
[16] M.N. Dean, R. Shahar, The structure-mechanics relationship and the response to load of the acellular bone of neoteleost fish: a review, J. Appl. Ichthyol. 28 (2012) 320–329.
[17] A. Atkins, N. Reznikov, L. Ofer, A. Masic, S. Weiner, R. Shahar, The three-dimensional structure of anosteocytic lamellated bone of fish, Acta Biomater. 13 (2015) 311–323.
[18] G.V. Lauder, E.G. Drucker, Morphology and experimental hydrodynamics of fish fin control surfaces, IEEE J. Ocean. Eng. 29 (2004) 556–571.
[19] A. Kolliker, On the different types in the microscopic structure of the skeleton of osseous fishes, Proc. R. Soc. Lond. 9 (1857) 656–668.
[20] S. Kranenbarg, T. van Cleynenbreugel, H. Schipper, J. van Leeuwen, Adaptive bone formation in acellular vertebrae of sea bass (Dicentrarchus labrax L.), J. Exp. Biol. 208 (2005) 3493–3502.
[21] M.L. Moss, Studies of the acellular bone of teleost fish, Cells Tiss Organs 46 (1961) 343–362.
[22] P.E. Witten, A. Huysseune, T. Franz-Odendaal, T. Fedak, M. Vickaryous, A. Cole, B.K. Hall, Acellular teleost bone: primitive or derived, dead or alive? Palaeontol. Assoc. Newslett. 55 (2004) 37–41.
[23] G.V. Lauder, L.E. Lanyon, Functional anatomy of feeding in the bluegill sunfish, Lepomis macrochirus: in vivo measurement of bone strain, J. Exp. Biol. 84 (1980) 33–55.
[24] M.L. Moss, Osteogenesis of acellular teleost fish bone, Am. J. Anat. 108 (1961) 99–109.
[25] R.E. Weiss, N. Watabe, Studies on the biology of fish bone. III. Ultrastructure of osteogenesis and resorption in osteocytic (cellular) and anosteocytic (acellular) bones, Calcif. Tissue Int. 28 (1979) 43–56.
[26] S. Ekanayake, B.K. Hall, Ultrastructure of the osteogenesis of acellular vertebral bone in the Japanese medaka, Oryzias-Latipes (Teleostei, Cyprinidontidae), Am. J. Anat. 182 (1988) 241–249.
[27] S. Ekanayake, B.K. Hall, The development of acellularity of the vertebral bone of the Japanese Medaka, Oryzias-Latipes (Teleostei, Cyprinidontidae), J. Morphol. 193 (1987) 253–261.
[28] A. mirone, E. Brun, E. Gouillart, P. Tafforeau, J. Kieffer, PyHST2: an hybrid distributed code for high speed tomographic reconstruction with iterative reconstruction and a priori knowledge capabilities, Nuclear Inst and Methods B 324 (2014) 41–48.
[29] Y. Shwartz, E. Zelzer, Nonradioactive in situ hybridization on skeletal tissue sections, Methods Mol. Biol. 1130 (2014) 203–215.
[30] W. Dong, D.E. Hinton, S.W. Kullman, TCDD disrupts hypural skeletogenesis during medaka embryonic development, Toxicol. Sci. 125 (2012) 91–104.
[31] J. Weigele, T.A. Franz-Odendaal, Functional bone histology of zebrafish reveals two types of endochondral ossification, different types of osteoblast clusters and a new bone type, J. Anat. 229 (2016) 92–103.
[32] P.E. Witten, M.P. Harris, A. Huysseune, C. Winkler, Small teleost fish provide new insights into human skeletal diseases, in: H.W. Detrich, IIIM. Westerfield, L.I. Zon (Eds.), Methods in Cell Biology, Elsevier Ltd, 2016, pp. 321–346.
[33] P.E. Witten, A. Huysseune, A comparative view on mechanisms and functions of skeletal remodelling in teleost fish, with special emphasis on osteoclasts and their function, Biol. Rev. 84 (2009) 315–346.
[34] J.Y. Sire, F. Meunier, Typical tubules in the acellular bone of gilthead sea bream Sparus aurata (Teleostei: Perciformes: Sparidae), Cah. Biol. Mar. 58 (2017) 467–474.
[35] Y. Lu, S.A. Kamel-El Sayed, K. Wang, L.M. Tiede-Lewis, M.A. Grillo, P.A. Veno, V. Dusevich, C.L. Phillips, L.F. Bonewald, S.L. Dallas, Live imaging of type I collagen assembly dynamics in osteoblasts stably expressing GFP and mCherry-tagged collagen constructs, J. Bone Miner. Res. 33 (2018) 1166–1182.
[36] N. Reznikov, R. Almany-Magal, R. Shahar, S. Weiner, Three-dimensional imaging of collagen fibril organization in rat circumferential lamellar bone using a dual beam electron microscope reveals ordered and disordered sub-lamellar structures, Bone 52 (2013) 676–683.
[37] N. Reznikov, R. Shahar, S. Weiner, Three-dimensional structure of human lamellar bone: the presence of two different materials and new insights into the hierarchical organization, Bone 59 (2013) 1–12.
[38] Y. Ben-Zvi, N. Reznikov, R. Shahar, S. Weiner, 3D architecture of trabecular bone in the pig mandible and femur: inter-trabecular angle distributions, Front. Mater. 4 (2017) 315–329.
[39] R.A. Magal, N. Reznikov, R. Shahar, S. Weiner, Three-dimensional structure of minipig fibrolamellar bone: adaptation to axial loading, 186 (2014) 253–264.
[40] J. Laerm, The development, function, and design of amphicoelous vertebrae in teleost fishes, Zool. J. Linnean Soc. 58 (1976) 237–254.
[41] N.C. Bird, P.M. Mabee, Developmental morphology of the axial skeleton of the zebrafish, *Danio rerio* (Ostariophysi: Cyprinidae), Dev. Dyn. 228 (2003) 337–357.
[42] M. Kerschnitzki, P. Kollmannsberger, M. Burghammer, G.N. Duda, R. Weinkamer, W. Wagermaier, P. Fratzl, Architecture of the osteocyte network correlates with bone material quality, J. Bone Miner. Res. 28 (2013) 1837–1845.
[43] F. Repp, P. Kollmannsberger, A. Roschger, A. Berzlanovich, G.M. Gruber, P. Roschger, W. Wagermaier, R. Weinkamer, Coalignment of osteocyte canaliculi and collagen fibers in human osteonal bone, J. Struct. Biol. 199 (2017) 1–28.
[44] M. Kerschnitzki, W. Wagermaier, P. Roschger, J. Seto, R. Shahar, G.N. Duda, S. Mundlos, P. Fratzl, The organization of the osteocyte network mirrors the extracellular matrix orientation in bone, J. Struct. Biol. 173 (2011) 303–311.
[45] S. Grotmol, H. Kryvi, K. Nordvik, G.K. Totland, Notochord segmentation may lay

down the pathway for the development of the vertebral bodies in the Atlantic salmon, Anat. Embryol. 207 (2003) 263–272.
[46] S. Grotmol, K. Nordvik, H. Kryvi, G.K. Totland, A segmental pattern of alkaline phosphatase activity within the notochord coincides with the initial formation of the vertebral bodies, J. Anat. 206 (2005) 427–436.
[47] E. Ytteborg, J. Torgersen, G. Baeverfjord, H. Takle, Morphological and molecular characterization of developing vertebral fusions using a teleost model, BMC Physiol. 10 (2010) 13.
[48] V.T. Carpentier, J. Wong, Y. Yeap, C. Gan, P. Sutton-Smith, A. Badiei, N.L. Fazzalari, J.S. Kuliwaba, Increased proportion of hypermineralized osteocyte lacunae in osteoporotic and osteoarthritic human trabecular bone: implications for bone remodeling, Bone 50 (2011) 688–694.
[49] T. Rolvien, F.N. Schmidt, P. Milovanovic, K.J.X. hn, C. Riedel, S. Butscheidt, K.P.X. schel, A. Jeschke, M. Amling, B.X.R. Busse, Early bone tissue aging in human auditory ossicles is accompanied by excessive hypermineralization, osteocyte death and micropetrosis, Sci. Rep. 8 (2018) 1–11.